CHEMISTRY OF MATERIALS
Cite This: Chem. Mater. XXXX, XXX, XXX−XXX
Article
pubs.acs.org/cm

Synthesis and Electronic Structure of a 3D Crystalline Stack of MXene-Like Sheets

Daniel L. Druffel,[†] Matthew G. Lanetti,[†] Jack D. Sundberg,[†] Jacob T. Pawlik,[†] Madeline S. Stark,[†] Carrie L. Donley,[‡] Lauren M. McRae,[†] Katie M. Scott,[†] and Scott C. Warren*[,†,¶]

[†]Department of Chemistry, University of North Carolina at Chapel Hill, Chapel Hill, North Carolina 27599, United States
[‡]Chapel Hill Analytical and Nanofabrication Laboratory (CHANL), University of North Carolina at Chapel Hill, Chapel Hill, North Carolina 27599, United States
[¶]Department of Applied Physical Sciences, University of North Carolina at Chapel Hill, Chapel Hill, North Carolina 27599, United States

Supporting Information

ABSTRACT: Despite the interest in MXenes in the past decade, MXenes are often highly disordered, which can complicate their study and use. For example, nearly all MXenes have a random mixture of surface terminations (−O, −OH, −F). In addition, restacked 3D films have turbostratic disorder and often contain ions, solvent, and other species in between their layers. Here, we report Y_2CF_2, a layered crystal with a unit cell isostructural to a MXene, in which layers are capped only by fluoride anions. We directly synthesize the 3D crystal through a high-temperature solid-state reaction, which affords the 3D crystal in high yield and purity and ensures that only fluoride ions terminate the layers. We characterize the crystal structure and electronic properties using a combination of experimental and computational techniques. We find that relatively strong electrostatic interactions bind the layers together into a 3D crystal and further find that the lack of orbital overlap between layers gives rise to a description of Y_2CF_2 as slabs of MXene-like sheets electrically insulated from one another. Therefore, we consider Y_2CF_2 as a pure 3D crystalline stack of MXene-like sheets. In addition, Y_2CF_2 is the first transition metal carbide fluoride experimentally synthesized. We hope this work inspires further exploration of transition metal carbide fluorides, which are potentially a large and useful class of compositions.

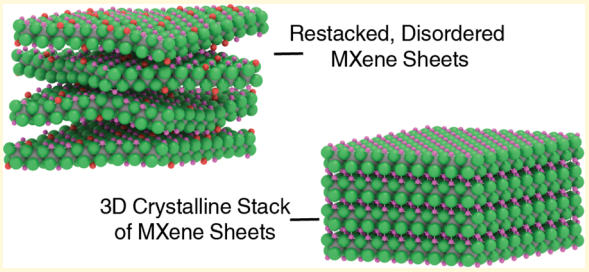

INTRODUCTION

Research into layered and 2D metal carbides such as MXenes has rapidly grown[1] due to their remarkable properties and applications in electronic,[2,3] sensing,[4,5] and energy storage devices.[6,7] Despite the interest in MXenes in the past decade, MXenes are often highly disordered, which can complicate their study and use. For example, nearly all MXenes have a random mixture of surface terminations (−O, −OH, −F). In addition, restacked 3D films of MXenes have turbostratic disorder[8] and often contain ions, solvent, and other species in between their layers.[9] The presence of multiple surface terminations on MXene sheets and disorder in their restacking owes to their usual synthesis, in which HF etches a MAX phase (M = metal; A = Al, Ga, Si, In; and X = C, N) with aqueous HF.[10] Indeed, the only reported MXene with a single surface moiety (−Cl) and without oxygen was prepared through etching a MAX phase in $ZnCl_2$ melts at elevated temperatures.[11]

Given the general interest in MXenes, it is remarkable that no pure (i.e., no −O, −OH) transition metal carbide fluoride has been reported. Of the transition metals, only Ti,[11] Y,[12−19] Sc,[12,20−24] Zr,[12,25,26] and W[27] have been studied as pure metal carbide halides and none as fluorides, leaving a large void in our knowledge of ternary phase diagrams. Our efforts in this work are to synthesize the first transition metal carbide fluoride and to highlight a largely unexplored class of compositions that may find utility in optoelectronics.

Here we report Y_2CF_2, a layered crystal with a unit cell isostructural to a 2D MXene, in which layers are capped only by fluoride anions. Relatively strong electrostatic interactions bind the layers together into a 3D crystal. Therefore, we consider Y_2CF_2 as a pure 3D crystalline stack of MXene-like sheets. Instead of the etching approach, we describe an alternative synthetic method. We directly synthesize the 3D crystal through a high-temperature solid-state reaction in the absence of air and water. The synthesis affords the 3D crystal in high yield and purity and ensures that only fluoride ions terminate the layers. This allows us to identify several useful

Received: September 10, 2019
Revised: November 9, 2019
Published: November 11, 2019

DOI: 10.1021/acs.chemmater.9b03722
Chem. Mater. XXXX, XXX, XXX−XXX

properties of Y_2CF_2: an indirect band gap of 1.6 eV, a direct band gap of 1.9 eV, and a small ionization potential of 3.8 eV. In addition, the crystals have modest charge transport properties, with an electron effective mass of 2.0 m_e and a hole effective mass of 4.0 m_e. This realization of a 3D crystalline stack of MXene-like sheets will enable a comparison to their 2D MXene counterparts to better understand the influence of disorder and surfaces on their optoelectronic properties.

EXPERIMENTAL SECTION

Synthesis of Y_2CF_2. Y_2CF_2 was synthesized by the solid state reaction of YF_3 (Sigma-Aldrich, granules, 0.09% oxygen, <0.02% Cd, Co, Cr, Fe, Hg, Mn, and Pb each) with Y metal (Alfa Aesar, ~40 mesh powder, 99.6% (REO)) and graphite (Sigma-Aldrich, ~100 mesh flakes, 99.9%). The reagents were ground into a fine powder in a stoichiometric ratio (total mass of a typical batch: 0.5−1.0 g) and pressed into a pellet under ~0.56 GPa of pressure using a hydraulic press. The pellet was welded inside an ampule made of tantalum (Ta) metal. To fashion an ampule, a Ta cap was hammered into Ta tubing and sealed in argon by welding the cap and tubing together with an electric arc. The Ta tubing, 99.95% Ta seamless tubing, was purchased from Eagle Alloys in a 1 cm diameter and cut to 5 cm lengths. The caps were made of the same Ta. After welding the reagents inside a Ta ampule, the Ta ampule was sealed in a fused quartz ampule under 1 mbar Ar. Then the vessel was placed in a Lindberg Blue M tube furnace and heated to 1513 K at a ramp rate of 10 K/min. The temperature was held at 1513 K for 3 days, then cooled to 1273 K over 10 h, then to 1073 K over 5 h, and to room temperature over 5 h. The ampule was then brought into the glovebox and opened with a pipe cutter. The pellet remained intact through the reaction. Vibrant green crystals grew on the surface of the pellet. The pellet revealed homogeneous green crystals throughout when broken apart. For some experiments, products were ball-milled for 15 min to reduce particle size. All materials were stored in a glovebox with an argon atmosphere (oxygen < 0.01 ppm), and all synthetic steps were carried out under an argon atmosphere.

Material Characterization. Samples were maintained under an inert atmosphere during transport and loading procedures, unless otherwise stated. Powdered samples of Y_2CF_2 were characterized by X-ray diffraction (XRD) at room temperature in a capillary transmission geometry across a range of 20−150° using Cu Kα (λ = 1.54056 Å) in a Rigaku Smartlab diffractometer. A reference scan was run with silicon powder (a = 5.430 Å) as an internal standard. The peak positions were not shifted as the height of the sample was already correct. The patterns were indexed using Treor[28] implemented in the Match! software.[29] The patterns were refined using the PDXL software from Rigaku. Thin films were characterized by X-ray photoemission spectroscopy (XPS) using a Kratos Axis Ultra Delay-Line Detector spectrometer with a monochromatic Al Kα source. For these measurements, the powder was pressed into indium substrates. High resolution XPS data were collected at a pass energy of 20 eV, and a charge neutralizer was used for charge compensation. All data were corrected to the C 1s peak at 284.6 eV. The samples were imaged using a Hitachi S-4700 cold cathode field emission SEM at an accelerating voltage of 2 kV with an Oxford energy-dispersive X-ray spectroscopy (EDS) detector. An accelerating voltage of 20 kV was used for EDS measurements. Samples were loaded onto the SEM sample holders in the glovebox and transported to the instrument under inert atmosphere; however, the samples were exposed to air for a few seconds during the transfer into the air lock of the instrument. UV−vis spectroscopy was performed in a transmission geometry through thin (~0.5 mm thick) discs made of mixtures of Y_2CF_2 and KBr. The Y_2CF_2 powder was diluted with spectroscopic grade KBr, ground finely in a ball mill until homogeneous, and then pressed into discs using a hydraulic press. The background due to scattering from KBr was subtracted by pressing films of KBr of varying thicknesses to estimate its effective attenuation as a function of thickness and subtracting a weighted fraction from the acquired spectra. The spectra were collected using a Cary 5000 UV−vis spectrometer with the DRA-2500 internal integrating sphere accessory. The reflection spectra of Y_2CF_2 particles from 400−850 nm were obtained using a Craic UV−vis−NIR microspectrophotometer with a polychromatic Xe source and an EC Epiplan Neofluar LD objective with an N.A. of 0.55. The aperture size was 14.7 × 14.7 μm except where noted.

DFT Calculations. Density functional theory (DFT) calculations were performed using the CASTEP[30] code with plane-wave basis set approximations. To describe core electrons, ultrasoft pseudopotentials[31] were used with a cutoff energy of 600 eV. For this cutoff energy, calculations were convergent with $dE_{tot}/d \ln E_{cut}$ less than 0.01 meV/atom. Geometry optimizations of all structures were first performed. A GGA PBE-sol functional[32] was used for the exchange-correlation contribution to total energy, and Tkatchenko and Scheffler's correction[33] was used to account for long-range dispersion forces for all calculations except where noted. A Monkhorst−Pack grid[34] of 16 × 16 × 8 k-points was used, and structures were optimized using a BFGS algorithm with a convergence tolerance of 5.0×10^{-7} eV/atom for energy, 0.01 eV/Å for max force, 0.02 GPa for max stress, and 5.0×10^{-4} Å for max displacement. The "thin-slab approach"[35] was used to calculate the ionization potential of bulk Y_2CF_2. For the calculations of ionization potential, a denser k-point mesh (32 × 32 × 16) was used. To prevent self-interactions between periodic images, a 12 Å vacuum space was included in the z-direction. The band gap and density of states were calculated using the HSE06 functional[36] with norm-conserving pseudopotentials,[37] a cutoff energy of 850 eV, and a k-point mesh of 32 × 32 × 16. The fixed-composition USPEX calculation was carried out via four serial geometry optimizations of each candidate structure. The geometry optimizations utilized the GGA PBE functional with increasing quality, where the fourth and final optimizations were converged to 5×10^{-5} eV/atom using a cutoff energy of 440 eV. For accurate comparison of candidate stabilities, geometry optimizations were followed by a single, higher-quality energy calculation converged to 5×10^{-6} eV/atom deemed sufficient to isolate reasonable Y_2CF_2 structure types. The search identified the minimum-energy structure from among ~400 candidates tested across eight generations.

RESULTS AND DISCUSSION

Synthesis and Crystal Structure. We combined yttrium, carbon, and fluorine in a stoichiometry of Y_2CF_2 at 1240 °C in sealed tantalum ampules according to the following reaction:

$$4Y + 3C + 2YF_3 \rightarrow 3Y_2CF_2 \quad (1)$$

The product is a pellet of beautiful green crystals (Figure 1a) that easily grinds into a powder (Figure 1b). Unfortunately, the synthesized crystals were too small and intergrown to perform single-crystal XRD measurements. Therefore, we combined two independent approaches to determine the crystal structure.

First, we performed powder XRD experiments of the product and obtained a diffraction pattern (Figure 1c), which indexed as a trigonal crystal structure with space group $P\bar{3}m1$-D_{3d}. Then, we refined the pattern by the Rietveld method[38] (Table 1). The analysis confirms that the trigonal space group $P\bar{3}m1$ is a good fit, with lattice constants a = 3.6651(3) Å and c = 6.29697(7) Å at room temperature (Figure 1c, Table 1). To show unambiguously that Y_2CF_2 is a layered structure, we also performed a measurement beginning at lower angles to capture reflections from the {00l} set of planes, including that from the (001) plane at 14.05° (Figure S1).

Independently, we used an evolutionary search algorithm, USPEX,[39] to explore computationally the stability of crystal structures for the composition Y_2CF_2. The algorithm computes the enthalpy of hundreds of candidate crystal structures and

DOI: 10.1021/acs.chemmater.9b03722
Chem. Mater. XXXX, XXX, XXX−XXX

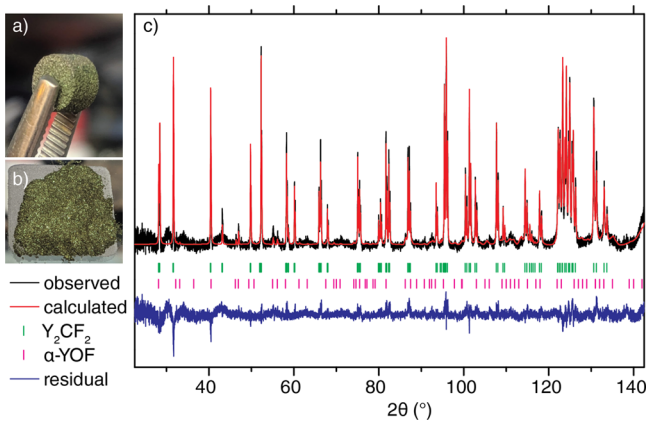

Figure 1. (a) Photograph of a pellet of Y_2CF_2 as synthesized. (b) Photograph of Y_2CF_2 ground in a mortar and pestle into a powder. (c) Observed, calculated, and residual profiles for Y_2CF_2 at 300 K measured on a Rigaku Smartlab diffractometer with a Cu Kα source, λ = 1.5406 Å. The pattern was refined to two phases, a Y_2CF_2 phase and an α-YOF phase (space group $P4/nmm$, a = 3.922 (2) Å, c = 5.409 (4) Å), which made up less than 4% by mole of the sample. Vertical tick marks indicate calculated reflection positions. The broad maxima in the background are due to diffuse scattering from the quartz ampule.

uses similarities in bond distances, coordination, symmetry, and a number of other identifiers to find the most stable phase for a given composition. Using the algorithm, we found that the $P\bar{3}m1$ structure is the most enthalpically favorable phase for the composition Y_2CF_2, in agreement with our diffraction experiments. The closest metastable phase is 46 meV/atom higher in energy than that of the $P\bar{3}m1$ structure. We then performed a geometry optimization calculation on the $P\bar{3}m1$ structure using the PBEsol[32] functional, which yielded lattice constants very close to the experimental values (1.6% shorter in a and 0.8% shorter in c, Figure 2b).

We also note that many yttrium compounds are isostructural to gadolinium and holmium compounds (e.g., YOCl, YCl_3, YF_3) because of the similarity in the crystallographic ionic radius of Y (104 pm)[40] to that of Gd and Y (108 and 104 pm, respectively).[40] In support of our indexing, we found known gadolinium and holmium compounds (Gd_2CF_2[41] and Ho_2CF_2[42]) isostructural to Y_2CF_2 with similar lattice constants.

The crystal structure of Y_2CF_2 (Figure 2a) is similar to that of MXenes. Six Y cations octahedrally coordinate each carbon atom, and the octahedra (Figure 2c) form into a two-dimensional layer, just like the 2D Ti_2C (−O, −OH, −F) MXene.[43] However, in the Y_2CF_2 structure, each Y cation also coordinates to four F anions, forming face-capped octahedra (Figure 2b). Thus, in Y_2CF_2, double layers of fluoride ions bind adjacent metal−carbide layers forming a crystalline 3D stack of MXene-like sheets.

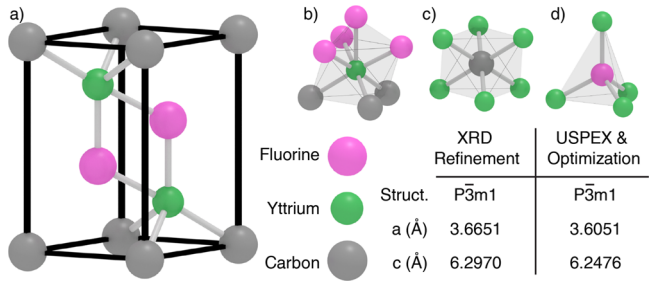

Figure 2. (a) Crystal structure, (b−d) bonding polyhedra, and lattice constants for Y_2CF_2. The crystal structure and lattice constants were obtained independently from two methods: (1) experimental synthesis and Rietveld refinement of X-ray diffraction data and (2) USPEX, a DFT-based search algorithm to find the most stable crystal structure for a given composition. After using USPEX to identify the structure, the structure was optimized using the PBEsol functional as described in the Experimental Section.

Naturally, we became interested in the interlayer bonding of Y_2CF_2, which is distinct from the 2D nature of MXenes. Each F coordinates to four Y with four nearly symmetric distances (Figure 3c), three to the Y in the adjacent layer (2.408 Å) and

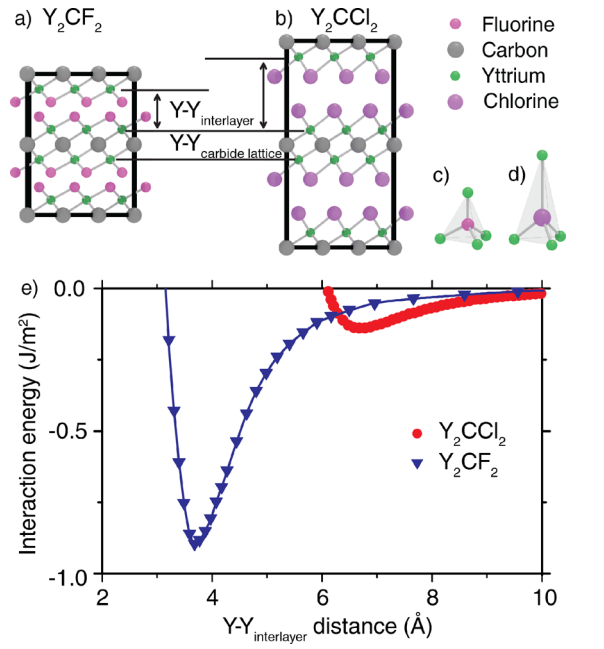

Figure 3. Comparison of the crystal structure of (a) Y_2CF_2 to (b) Y_2CCl_2 showing the unit cells along the [100] axis, the tetrahedral bonding polyhedron for yttrium and fluorine in (c) Y_2CF_2 and the same polyhedron drawn for (d) Y_2CCl_2 with the elongated Y−Cl distance in the z-direction, and (e) the interlayer binding energy for Y_2CF_2 (blue) and Y_2CCl_2 (red) calculated using the PBEsol functional.

Table 1. Final Parameters and R Factors for Y_2CF_2 at 300 K[a]

atom	site	symmetry	X	Y	Z	B (Å^2)	N	Occupancy
Y	2d	$3m$	13	23	0.21450(10)	0.526(12)	2	1.00(1)
C	1a	$\bar{3}m$	0	0	0	0.1(4)	1	0.93(3)
F	2d	$3m$	13	23	0.0.6031(5)	0.555(11)	2	1.00(6)

[a]Space group $P\bar{3}m1$. a = 3.6651 (3) Å, c = 6.29697 (7) Å. Volume = 73.2536 Å^3, density = 4.394 g cm^{-3}. Rietveld analysis standard agreement indices are the residual factor R_p = 2.5%, the weighted residual factor R_{wp} = 4.97%, and the goodness of fit factor S = 1.96. U, V, W (deg^2): 0.000, −0.021, 0.00.

DOI: 10.1021/acs.chemmater.9b03722
Chem. Mater. XXXX, XXX, XXX−XXX

one to the Y in the opposite layer at an only slightly elongated distance (2.447 Å) (Table 2). This suggests that the interlayer bonding is relatively strong and highly ionic in nature.

Table 2. Interatomic Distances in the Crystal Structure of Y_2CF_2, Determined by the Refinement of Powder X-ray Diffraction Data[a]

atom	interatomic distances (Å)
Y–Y	3.4315(2), 3.6651(3), 4.1720(1)
Y–F	2.4077(3), 2.4470(1)
F–F	2.4827(7)
Y–C	2.5104(6)
F–C	3.2747(6)

[a]All distances are reported in Å.

This electrostatic interlayer bonding contrasts with that of other known layered metal carbide halides. For example, in Y_2CCl_2,[12] which shares the same crystal structure (Figure 3b), Cl coordinates only to three Y, all in the adjacent layer (2.755 Å). The distance to the Y in the opposite layer is nearly double (4.770 Å), far too long for any Y–Cl bonding interaction (Figure 3d). Instead, the primary interlayer interactions in Y_2CCl_2 are weak van der Waals forces.

Using the PBEsol functional, we calculated the binding energy—the energy difference between the equilibrium bulk separation and the state in which the planes are separated by an infinite distance, as approximated by a 15 Å-thick vacuum-gap (Figure 3e). The binding energy for Y_2CF_2 is 0.90 J/m^2, over 6× that of Y_2CCl_2 (0.14 J/m^2) and 3× that of graphite (0.34 J/m^2).[44] Electrostatic interactions between the F anion and the Y cation likely account for the greater binding energy. This leads us to conclude that Y_2CF_2 is an ionic crystal in the out-of-plane direction. Still, the binding energy of Y_2CF_2 is less than that of other layered crystals that have been exfoliated successfully into 2D flakes, for example, Ca_2N (1.11 J/m^2).[45] These calculations suggest that it may be possible to exfoliate Y_2CF_2 into 2D flakes, although with somewhat greater difficulty than van der Waals crystals like Y_2CCl_2 or graphite.

Composition and Purity. We sought to confirm the composition of our sample, as some metal carbides can sustain a variety of nonstoichiometric compositions. We used EDS to quantify the amount of yttrium and fluorine (Figure S3) and measured a ratio of 1:0.98 ± 0.05 Y:F in agreement with the stoichiometry of Y_2CF_2. These results also agree with the refinement from powder X-ray measurements, which yielded an occupancy of 1.00 ± 0.01 and 1.00 ± 0.06 for yttrium and fluorine, respectively, in each of their 2d sites (Table 1). Unfortunately, our EDS instrument does not quantify carbon reliably because the signal is obscured by electronic noise. Therefore, we quantified carbon by refining the occupancy of the carbon site during the Rietveld refinement, which revealed that only 93 ± 3% are occupied. We conclude that the composition Y_2CF_2 represents the synthesized phase, though the real structure has carbon vacancies, $Y_2C_{0.93}F_2$.

Electronic Structure of Y_2CF_2. To investigate the effect of interlayer ionic bonding on the electronic structure of stacked MXene-like sheets, we examined the material's optoelectronic properties using both experiment and computation. First, we performed transmission measurements to quantify the absorption coefficient (Figure S5a). We observe a gradual increase in absorption beginning at ~775 nm (1.6 eV), which we attribute to the band gap. The absorption increases and plateaus from 400 to 550 nm at a magnitude of 3.4 × 10^4 cm^{-1}. The absorption coefficient has local maxima at 340 nm and again at 240 nm, though the local maximum at 240 nm is obscured by the attenuation of our quartz substrate. Our

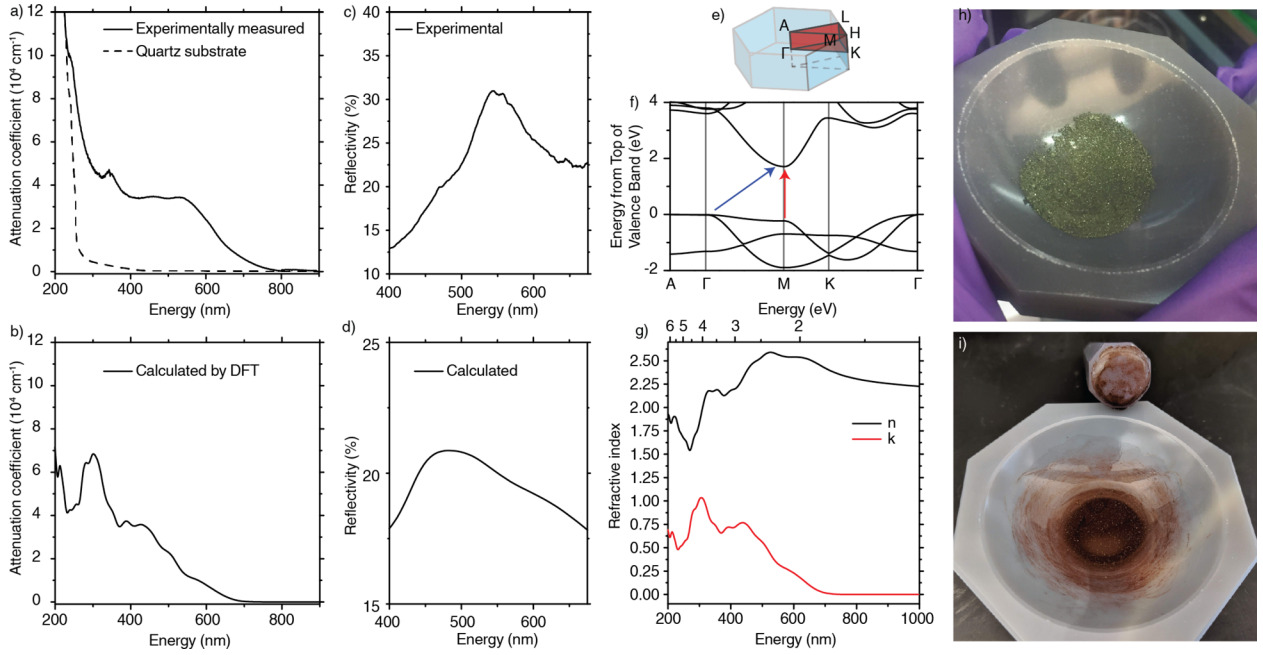

Figure 4. Optical properties of Y_2CF_2. Attenuation coefficient (a) measured experimentally, which does not include the contribution from the quartz substrate; however, at wavelengths shorter than 250 nm the signal was dominated and obscured by that of the quartz. (b) Attenuation coefficient calculated by DFT. Reflectivity (c) measured experimentally and (d) calculated by DFT. (e) First Brillouin zone for $Y_2CF\Gamma$ with the irreducible Brillouin zone highlighted in red and (f) electronic band structure where the M–Γ vector runs along (010), while the Γ–A vector runs along (001). (g) Optical constants, *n* and *k*, calculated by DFT. Photograph of (h) green Y_2CF_2 before grinding and (i) red Y_2CF_2 after grinding.

DOI: 10.1021/acs.chemmater.9b03722
Chem. Mater. XXXX, XXX, XXX–XXX

computational model shows a gradual increase in absorption beginning at 700 nm (1.7 eV; Figure 4b), in excellent agreement with our experimental measurements. The absorption coefficient plateaus from 375 to 450 nm at a magnitude of 3.4×10^4 cm^{-1}, nearly identical to our experiment. Finally, the model predicts peaks at 300 and 210 nm, red-shifted only 40 nm from our experimental data.

Next, we performed specular-reflectance measurements on single facets of individual Y_2CF_2 crystals (Figure S5) using a microspectrophotometer. To obtain a representative spectrum, we averaged the spectra from individual crystallites together (Figure 4c). The representative spectrum has a peak at 540 nm, corresponding to yellow-green light. To compare with our model of the electronic structure, we calculated the reflectivity for the bulk Y_2CF_2 (Figure 4d), which shows a single broad peak at 500 nm, again red-shifted only 40 nm from experiment. We do note that the intensity of the reflection in the experiment is roughly 50% larger than that in the computation. While the computation provides qualitative information, it does not consider all of the complexity of the real system (e.g., chemical differences at the surface, an interface with a changing dielectric, or the convolution of reflection and absorption events). Therefore, we attribute the difference in magnitude to these factors. Despite this difference, the model reproduces the major features of the experiment well.

We calculated the electronic band structure for the first Brillouin zone of Y_2CF_2, shown in Figure 4e,f. In agreement with our experimental measurements, we calculate that Y_2CF_2 is a semiconductor with an indirect gap of 1.7 eV (from Γ−M) and a direct gap of 1.9 eV (M−M; Figure 4f). From the band structure, we can understand that the low absorption coefficient at 700 nm (Figure 4a,b) is due to the indirect nature of the transitions and the low density of states in the conduction band. Moreover, we gain information about the band dispersion. The bottom of the conduction band has a parabolic band dispersion, which should correspond to a modest effective mass (2.0 m_e) for electrons in the conduction band. In contrast, the valence band is relatively flat giving rise to a higher hole effective mass (4.0 m_e). Interestingly, the band has almost no dispersion along the path Γ−A (Figure 4f) indicating very limited overlap of orbitals in the z-direction. This is likely due to the strong localization of electrons around the nucleus of the fluorine atoms, which separate layers of yttrium and carbon atoms. Therefore, the ionic bonding between MXene-like sheets effectively insulates the sheets from one another electronically, which will give rise to highly anisotropic optoelectronic properties.

Because of the excellent agreement between theory and experiment, we present the optical constants (Figure 4g), n and k, calculated using the HSE06 functional with confidence that the energy dependence of the optical constants and that the magnitude of k represent the synthesized Y_2CF_2. Due to the difference in magnitude between experiment and calculation, there is more uncertainty in the magnitude of n.

The electronic structure also explains an observation about the perceived color of Y_2CF_2. When we ground the green crystals (Figure 4g) in a glovebox in the absence of air or water, the material transforms into a red powder (Figure 4i). By examining the electronic structure, we conclude that the initially perceived green color is due to specular reflection of green light from flat crystalline surfaces, as evidenced by the peak in reflection at 540 nm in Figure 4c. By grinding the crystals into small particles, we destroy the flat surfaces and the specular reflection of green light. Once ground, absorption originating from the band gap at 775 nm dominates the apparent color of the material. To test this hypothesis, we ball milled the crystals to a fine powder with a particle size qualitatively determined as less than 5 μm (Figure S7). We confirmed, via powder XRD, that the crystal structure is preserved after ball milling (Figure S8). Then we measured the reflectance of the finely ground sample using a microspectrophotometer (Figure S9). We found that the peak at 540 nm, observed for the green crystals, was not present in the ball-milled sample.

Sensitivity to Oxygen. This understanding of Y_2CF_2's electronic structure also led us to explore its sensitivity to oxygen and water. We removed samples of crystalline Y_2CF_2 from the glovebox, exposing the crystals to air and water for one month. After two weeks, the once-green crystals appeared red (Figure S10). Examining the crystals in the microspectrophotometer in reflectance mode, we found that the peak at 540 nm corresponding to the green color was not present. Instead, we observe rainbow striping and periodic oscillating signals in the reflectance spectra (Figure S11), which are indicative of thin-film optical interference. The formation of a thin film on the surface of many semiconductors is commonly caused by a slow reaction with air or water, which forms a thin oxide coating.[46] Therefore, we suspected that Y_2CF_2 in air develops a thin film of an oxide or related species.

To test whether the Y_2CF_2 crystals react with oxygen or water, we performed X-ray photoemission spectroscopy (XPS) on crystals exposed to air for one week and on crystals kept in the glovebox. We examined the yttrium 3d, carbon 1s, fluorine 1s, and carbon 1s core electron binding energies (Table 3). For the sample exposed to air for 1 week, we observed a single peak at a binding energy of 684.8 eV (Figure 5a) corresponding to the F 1s core binding energy, in agreement with the binding

Table 3. X-ray Photoemission Spectra from Y_2CF_2 Exposed to Air for 1 Week, after Sputtering, and from Y_2CF_2 Kept in an Ar-Filled Glovebox (oxygen < 0.01 ppm) for 1 Week[a]

sample	atom	core	binding energy[b]	fwhm	atomic %
air-exposed	Y	$3d^5/_2$	157.6	1.56	21.3
	C_{adv}	1s	284.6,[b] 286.3	1.33, 2.24	17.1
	$C_{carbonate}$	1s	289.4	1.63	7.9
	F	1s	684.8	1.81	10.5
	O	1s	531.2	1.88	43.2
air-exposed sputtered	Y	$3d^5/_2$	157.6	2.58	33.8
	C_{adv}	1s	284.6[b], 286.0	1.67, 1.76	5.3
	$C_{carbonate}$	1s	289.9	1.57	1.9
	F	1s	685.0	2.11	16.9
	O	1s	531.3	3.91	42.1
glovebox	Y	$3d^5/_2$	155.3	1.27	6.7
	Y	$3d^5/_2$	157.6	2.19	19.4
	$C_{carbide}$	1s	279.6	1.04	4.5
	C_{adv}	1s	284.6,[b] 286.3	1.25, 1.55	27.4
	F	1s	684.4	1.75	18.8
	O	1s	531.2	2.33	27.1

[a]All binding energies and full-width at half-maximum values given in eV. [b]All binding energies were referenced to adventitious carbon (284.6 eV).

DOI: 10.1021/acs.chemmater.9b03722
Chem. Mater. XXXX, XXX, XXX−XXX

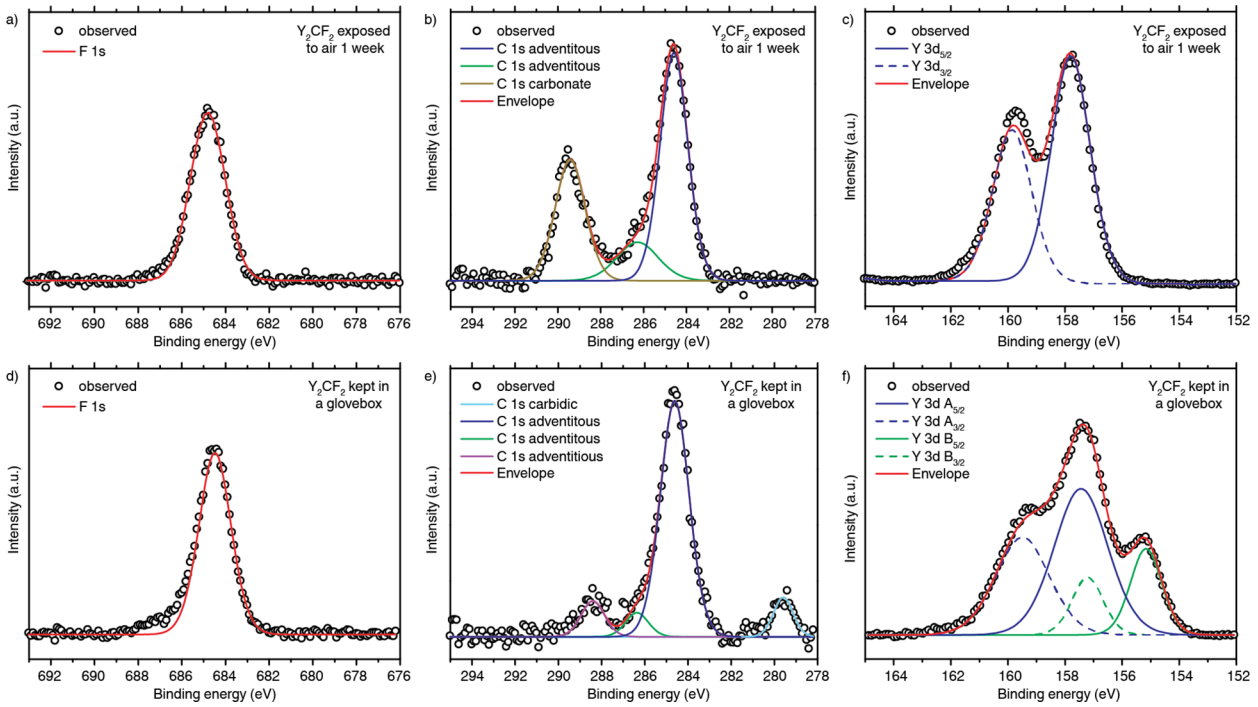

Figure 5. X-ray photoemission spectra from Y_2CF_2 exposed to air for 1 week for the (a) fluorine 1s, (b) carbon 1s, and (c) yttrium 3d core electron binding energies. X-ray photoemission spectra from Y_2CF_2 kept in a glovebox for the (d) fluorine 1s, (e) carbon 1s, and (f) yttrium 3d core electron binding energies.

energy of fluoride.[47] However, the Y:F ratio measured through XPS quantitative analysis is 1:0.5, suggesting a deficiency of fluorine at the surface. In the Y 3d spectrum we observe a doublet with a binding energy of 157.7 eV (Figure 5c). The position of this peak matches that of yttrium carbonate ($Y_2(CO_3)_3$)[48] and is too high to be the expected Y^{2+} oxidation state (~156 eV).[49] In addition, the spectrum of the carbon 1s core (Figure 5b) reveals two distinct peaks, one centered at 284.6 eV, which is adventitious carbon, and one centered at 289.4 eV, which matches that of a carbonate (Figure 5b).[50] Moreover, through quantitative XPS analysis, we measure the ratio of Y:O to be 1:2.1, which can only be explained by a carbonate, not Y_2O_3 or YOF. Therefore, the data suggest the surface of the sample exposed to air has oxidized, at least partially, to yttrium carbonate.

We attempted to clean the surface of the air-exposed sample by argon ion sputtering (Figure S12). Both the oxygen 1s and carbon 1s signals decrease in intensity relative to the yttrium (Table 3). The Y:O ratio decreases to 1:1.2. This suggests that the oxidation is a surface effect. For additional support of that hypothesis, we performed XRD measurements on the samples exposed to air (Figure S13). We found the crystal structure remained intact after exposure to air for 1−4 weeks, which supports the conclusion that the oxidation affects the surface and not the bulk of the sample.

For the sample kept in a glovebox, the sample was briefly exposed to air during the transfer into the XPS instrument. We attempted this measurement multiple times and found that the sample is prone to charging. Here, we present the data from the experiment that showed the least charging. The F 1s spectrum (Figure 5d) has a single peak at 684.4 eV similar to that of the air-exposed sample (Table 3). We attribute the small tail at higher binding energies in the F 1s spectrum to this charging. The carbon 1s spectrum (Figure 5e) shows one main peak, which we attribute to adventitious carbon (Table 3) and which we used to reference the data. Referencing to any other carbon peak yields unreasonable values for the peaks of other elements. In addition to the adventitious carbon, we observe a peak at a very low binding energy (279.6 eV). Carbidic carbon in similar materials, for example, Sc_2CCl_2 (281.8 eV),[12] TiC (281.5 eV),[51] ZrC (281.1 eV),[52] and HfC (280.8 eV),[52] gives rise to peaks at low binding energies, but none quite as low as what we observe here. Therefore, we considered that the signal could be due to other elements, which have signals at similar binding energies (Os 4d, Ru 3d, Sr 3p, Tb 4p, and Cl 2s). We rule out Os, Sr, Tb, and Cl because the XPS survey scan (Figure S14) reveals that the most intense peaks for these elements are absent (Os 4f at 50−55 eV,[53] Sr 3d and 3s at 130−135 and 357 eV, respectively,[54] Tb 4d at 150 eV,[55] and Cl 2p at 198−208 eV[56]). The most intense peak for Ru is the 3d peak, so we cannot rule out Ru directly. However, we have no reason to suspect the incorporation of Ru into our sample and its weaker peaks are absent (Ru 4s at 75 eV, Ru 3p at 463 eV, and Ru 3s at 586 eV).[57] Therefore, we assign the peak at 279.6 eV as carbidic carbon in Y_2CF_2, consistent with a highly reduced form of carbon. We also note that we do not observe the signal at higher binding energies of a carbonate species for the sample kept in the glovebox. Finally, in the Y 3d spectrum, we observe two distinct yttrium signals (Figure 5f). One contribution is from a reduced form of yttrium with a binding energy of 155.3 eV, and a second contribution is from an oxidized form of yttrium at 157.6 eV that matches that of the air-exposed sample. A reduced form of yttrium is consistent with our understanding of Y_2CF_2, in which we expect the Y adopts a 2+ oxidation state. The second contribution is broadened compared to the air-exposed sample possibly due to the small amount of charging present during the collection of data.

DOI: 10.1021/acs.chemmater.9b03722
Chem. Mater. XXXX, XXX, XXX−XXX

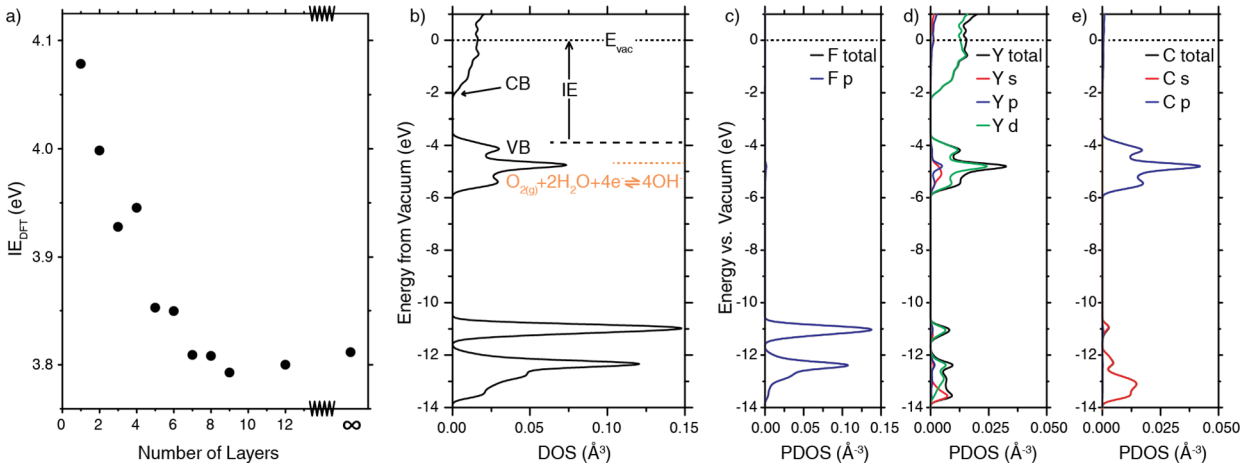

Figure 6. Band positions of Y_2CF_2 on an absolute scale. (a) Calculations of the ionization potential (IE) by DFT as described in the Experimental Section for increasingly thick slabs of Y_2CF_2, which plateau at a value of ~3.8 eV for a 12-layer slab and for a bulk crystal. (b) Density of states (DOS) of bulk Y_2CF_2 calculated by DFT referenced to vacuum energy using the calculated ionization potential, showing the valence band (VB) and conduction band (CB). The partial density of states for (c) fluorine, (d) yttrium, and (e) carbon in Y_2CF_2.

Therefore, we conclude that the surface of Y_2CF_2 oxidizes quickly during the brief transfer of the sample into the instrument and that the oxidation affects the reduced yttrium and carbidic carbon at the surface.

We return to the electronic structure to understand why Y_2CF_2 oxidizes in air. We combined several measurements and calculations to place the band edges of Y_2CF_2 on an absolute scale along with the reduction potentials of oxygen and water, which are likely redox couples.[46] DFT calculations gave the valence band edge (Figure 6a) and band gaps (Figure 4b,e), which are supported by our spectroscopic measurements (Figure 4a). The valence band edge is at a higher energy than the reduction potentials of oxygen and water, which explains why the material oxidizes. We gain further understanding of its reactivity through analysis of the partial density of states (PDOS), deconstructed into the elemental compositions and angular momentum (Figure 6c–e). The valence band consists of Y 4d and C 2p states. The C 2p states lie at high energies, and therefore the electrons occupying these states can be readily donated to oxygen and water, producing hydroxide. If this initial oxidation is not self-limiting, more highly oxidized products may form, such as yttrium carbonate. This mechanism is consistent with the XPS observations of fast partial oxidation to an oxide or hydroxide after a brief exposure to air and a subsequent slow oxidation to a more oxidized form.

In general, MXenes have been considered stable in air and water; however, growing evidence reveals that MXenes decompose over the course of a few days to a few weeks.[58−62] For example, Ti_3C_2 (−O, −OH, −F) decomposes to form TiO_2 in the presence of oxygen[58,61] and water.[60,63] In fact, the etching synthetic method, which uses strong oxidants like HF,[10] H_2O_2,[64] or HCl/LiF,[65] contributes to the oxidation, as evidenced by the formation of −O terminating moieties. The oxidation has consequences on the electronic structure.[66] For example, the work function of Ti_3C_2 (−O, −OH, −F) was predicted to vary from 1.9 to 6.2 eV depending on the surface terminations.[67] Moreover, the work function of MXenes with random surface moieties depends on the complex interplay between the different surface moieties and their local dipoles.[68]

In this context, Y_2CF_2 and crystalline stacked MXenes provide an opportunity. The uniform, single F− moiety of crystalline stacked MXenes could facilitate experiments to understand and control its surface oxidation. Although we have observed that Y_2CF_2 oxidizes in air, the material reported here is intrinsically oxygen-free, unlike the 2D MXenes synthesized by etching in aqueous HF. It therefore provides a reference for detecting changes in surface composition and surface properties. If this pristine 3D crystal can be exfoliated in water-free or oxygen-free conditions, it may also yield an unoxidized, pristine 2D MXene. In addition, the 3D crystalline form eliminates both the turbostratic disorder and the incorporation of solvent, ions, and other species between sheets found in restacked films of MXene sheets, which likely gives superior optoelectronic properties.

CONCLUSION

We have synthesized Y_2CF_2, a crystalline, 3D stack of MXene-like sheets capped exclusively by fluorine. Instead of the etching approach, we introduce a new synthetic method to directly synthesize the 3D crystal through a high-temperature solid-state reaction that ensures that only fluorine terminates the layers. Unlike MXenes, ionic bonds hold layers together. Interestingly, because the fluorine orbitals contribute to neither the valence band nor the conduction band, the fluorine layers electrically isolate the yttrium carbide layers from each other. This imparts to the 3D crystal 2D-like electronic transport and supports an understanding of these materials as a crystalline stack of MXene-like sheets. The valence band edge, made of Y 4d and C 2p states, sits at a high energy, affording reducing character, which makes the crystal sensitive to air but also suggests that the crystal could be useful in applications in electronics,[2,3] sensing,[4,5] and energy storage.[6,7]

ASSOCIATED CONTENT

Supporting Information

The Supporting Information is available free of charge at https://pubs.acs.org/doi/10.1021/acs.chemmater.9b03722.

Additional details regarding the synthesis and characterization of Y_2CF_2, ball-milled Y_2CF_2, and air-exposed Y_2CF_2; SEM and EDS data, XRD, and optical measurements of Y_2CF_2; and photographs of powders (PDF)

DOI: 10.1021/acs.chemmater.9b03722
Chem. Mater. XXXX, XXX, XXX−XXX

AUTHOR INFORMATION

Corresponding Author

*(S.C.W.) E-mail: sw@unc.edu.

ORCID

Daniel L. Druffel: 0000-0003-4340-4489
Matthew G. Lanetti: 0000-0001-9528-9174
Jack D. Sundberg: 0000-0001-5739-8919
Jacob T. Pawlik: 0000-0002-6704-2817
Madeline S. Stark: 0000-0002-0134-0774
Carrie L. Donley: 0000-0003-0906-306X
Lauren M. McRae: 0000-0002-0360-9626
Scott C. Warren: 0000-0002-2883-0204

Notes

The authors declare no competing financial interest.

ACKNOWLEDGMENTS

S.C.W. acknowledges support of this research by NSF Grant DMR-1905294. J.D.S, J.T.P., and M.S.S. acknowledge support by the NSF Graduate Research Fellowship under Grant DGE-1650114. This work was performed in part at the Chapel Hill Analytical and Nanofabrication Laboratory, CHANL, a member of the North Carolina Research Triangle Nanotechnology Network, RTNN, which is supported by the National Science Foundation, Grant ECCS-1542015, as part of the National Nanotechnology Coordinated Infrastructure, NNCI. The authors acknowledge the support of the Alliance for Molecular PhotoElectrode Design for Solar Fuels (AMPED) EFRC, an Energy Frontier Research Center funded by the U.S. Department of Energy, Office of Science, Office of Basic Energy Sciences, under Award Number DE-SC0001011, for access to a Cary 5000 UV−vis spectrometer with the DRA-2500 internal integrating sphere accessory instrumentation. The authors are also grateful to the Research Computing Center, University of North Carolina at Chapel Hill, for access to needed computing facilities to perform the computational studies reported in this work.

REFERENCES

(1) Naguib, M.; Mochalin, V. N.; Barsoum, M. W.; Gogotsi, Y. 25th anniversary article: MXenes: a new family of two-dimensional materials. *Adv. Mater.* **2014**, *26*, 992−1005.

(2) Zhao, M.-Q.; Ren, C. E.; Ling, Z.; Lukatskaya, M. R.; Zhang, C.; Van Aken, K. L.; Barsoum, M. W.; Gogotsi, Y. Flexible MXene/carbon nanotube composite paper with high volumetric capacitance. *Adv. Mater.* **2015**, *27*, 339−345.

(3) Li, R.; Zhang, L.; Shi, L.; Wang, P. MXene Ti_3C_2: an effective 2D light-to-heat conversion material. *ACS Nano* **2017**, *11*, 3752−3759.

(4) Kim, S. J.; Koh, H.-J.; Ren, C. E.; Kwon, O.; Maleski, K.; Cho, S.-Y.; Anasori, B.; Kim, C.-K.; Choi, Y.-K.; Kim, J.; Gogotsi, Y.; Jung, H.-T. Metallic $Ti_3C_2T_x$ MXene gas sensors with ultrahigh signal-to-noise ratio. *ACS Nano* **2018**, *12*, 986−993.

(5) Yu, X.-f.; Li, Y.-c.; Cheng, J.-b.; Liu, Z.-b.; Li, Q.-z.; Li, W.-z.; Yang, X.; Xiao, B. Monolayer Ti_2CO_2: a promising candidate for NH_3 sensor or capturer with high sensitivity and selectivity. *ACS Appl. Mater. Interfaces* **2015**, *7*, 13707−13713.

(6) Naguib, M.; Come, J.; Dyatkin, B.; Presser, V.; Taberna, P.-L.; Simon, P.; Barsoum, M. W.; Gogotsi, Y. MXene: a promising transition metal carbide anode for lithium-ion batteries. *Electrochem. Commun.* **2012**, *16*, 61−64.

(7) Liang, X.; Garsuch, A.; Nazar, L. F. Sulfur cathodes based on conductive MXene nanosheets for high-performance lithium−sulfur batteries. *Angew. Chem., Int. Ed.* **2015**, *54*, 3907−3911.

(8) Ghidiu, M.; Barsoum, M. W. The {110} reflection in X-ray diffraction of MXene films: Misinterpretation and measurement via non-standard orientation. *J. Am. Ceram. Soc.* **2017**, *100*, 5395−5399.

(9) Ren, C. E.; Hatzell, K. B.; Alhabeb, M.; Ling, Z.; Mahmoud, K. A.; Gogotsi, Y. Charge-and size-selective ion sieving through $Ti_3C_2T_x$ MXene membranes. *J. Phys. Chem. Lett.* **2015**, *6*, 4026−4031.

(10) Naguib, M.; Kurtoglu, M.; Presser, V.; Lu, J.; Niu, J.; Heon, M.; Hultman, L.; Gogotsi, Y.; Barsoum, M. W. Two-dimensional nanocrystals produced by exfoliation of Ti_3AlC_2. *Adv. Mater.* **2011**, *23*, 4248−4253.

(11) Lu, J.; et al. $Ti_{n+1}C_n$ MXenes with fully saturated and thermally stable Cl terminations. *Nanoscale Adv.* **2019**, *1*, 3680−3685.

(12) Hwu, S.-J.; Ziebarth, R. P.; von Winbush, S.; Ford, J. E.; Corbett, J. D. Synthesis and structure of double-metal-layered scandium, yttrium, and zirconium chloride carbides and nitrides, M_2Cl_2C and M_2Cl_2N. *Inorg. Chem.* **1986**, *25*, 283−287.

(13) Henn, R.; Schnelle, W.; Kremer, R.; Simon, A. Bulk superconductivity at 10 K in the layered compounds $Y_2C_2I_2$ and $Y_2C_2Br_2$. *Phys. Rev. Lett.* **1996**, *77*, 374−377.

(14) Ahn, K.; Kremer, R. K.; Simon, A.; Marshall, W. G.; Puschnig, P.; Ambrosch-Draxl, C. Influence of pressure on the structure and electronic properties of the layered superconductor $Y_2C_2I_2$. *J. Phys.: Condens. Matter* **2005**, *17*, S3121.

(15) Kauzlarich, S. M.; Hughbanks, T.; Corbett, J. D.; Klavins, P.; Shelton, R. N. Two extended metal chain compounds, yttrium iodide carbides (Y_4I_5C and $Y_6I_7C_2$). Synthesis, structure, properties, and bonding. *Inorg. Chem.* **1988**, *27*, 1791−1797.

(16) Kauzlarich, S. M.; Payne, M. W.; Corbett, J. D. $Y_{10}I_{13}C_2$: a novel compound with chains of both carbon-centered and empty clusters. *Inorg. Chem.* **1990**, *29*, 3777−3781.

(17) Schaloske, M. C.; Kienle, L.; Duppel, V.; Mattausch, H.; Simon, A. $SE_{19}(C)_{23}I_{34}$ (SE= Y, Gd): Verbindungen mit diskreten SE_6I_{12}-clustern und isolierten SE-atomen. *Z. Anorg. Allg. Chem.* **2009**, *1*, 188−195.

(18) Hinz, D.; Meyer, G. Crystal structure of yttrium carbide iodide (10−4−18), $[Y_{10}(C)_{22}]I_{18}$. *Z. Kristallogr. Cryst. Mater.* **1995**, *210*, 957−957.

(19) Simon, A.; Bäcker, M.; Henn, R.; Felser, C.; Kremer, R.; Mattausch, H.; Yoshiasa, A. Supraleitung in seltenerdmetall-carbidhalogeniden des typs $SE_2X_2C_2$. *Z. Anorg. Allg. Chem.* **1996**, *622*, 123−137.

(20) Jongen, L.; Mudring, A.-V.; Meyer, G. The molecular solid $Sc_{24}C_{10}I_{30}$: A truncated, hollow T4 supertetrahedron of iodine filled with a T3 supertetrahedron of scandium that encapsulates the adamantoid cluster Sc_4C_{10}. *Angew. Chem., Int. Ed.* **2006**, *45*, 1886−1889.

(21) Dudis, D. S.; Corbett, J. D.; Hwu, S. J. Synthesis, characterization, and crystal structures of two scandium cluster carbides and a boride, $Sc_7X_{12}C$ (X= I, Br) and $Sc_7I_{12}B$. *Inorg. Chem.* **1986**, *25*, 3434−3438.

(22) Hwu, S.-J.; Corbett, J. D. Metal-metal-bonded scandium cluster ($Sc_7Cl_{12}Z$) and infinite chain (Sc_4Cl_6Z) phases stabilized by interstitial boron or nitrogen (Z). *J. Solid State Chem.* **1986**, *64*, 331−346.

(23) Dudis, D. S.; Corbett, J. D. Two scandium iodide carbides containing dicarbon units within scandium clusters: $Sc_6I_{11}C_2$ and $Sc_4I_6C_2$. Synthesis, structure, and the bonding of dicarbon. *Inorg. Chem.* **1987**, *26*, 1933−1940.

(24) Hwu, S.-J.; Corbett, J. D.; Poeppelmeier, K. R. Interstitial atoms in metal-metal bonded arrays: The synthesis and characterization of heptascandium decachlorodicarbide, $Sc_7Cl_{10}C_2$, and comparison with the interstitial-free Sc_7Cl_{10}. *J. Solid State Chem.* **1985**, *57*, 43−58.

(25) Smith, J. D.; Corbett, J. D. Four zirconium iodide cluster phases centered by boron, aluminum, or silicon. *J. Am. Chem. Soc.* **1986**, *108*, 1927−1934.

(26) Smith, J. D.; Corbett, J. D. Stabilization of clusters by interstitial atoms. Three carbon-centered zirconium iodide clusters, $Zr_6I_{12}C$, $Zr_6I_{14}C$, and $MZr_6I_{14}C$ (M= K, Rb, or Cs). *J. Am. Chem. Soc.* **1985**, *107*, 5704−5711.

DOI: 10.1021/acs.chemmater.9b03722
Chem. Mater. XXXX, XXX, XXX−XXX

(27) Ströbele, M.; Meyer, H.-J. The new binary tungsten iodide $W_{15}I_{47}$. *Z. Anorg. Allg. Chem.* **2010**, *636*, 62−66.
(28) Werner, P.-E.; Eriksson, L.; Westdahl, M. TREOR, a semi-exhaustive trial-and-error powder indexing program for all symmetries. *J. Appl. Crystallogr.* **1985**, *18*, 367−370.
(29) Putz, H.; Brandenburg, K. *Match!-phase identification from powder diffraction*; Crystal Impact Software. http://www.crystalimpact.com/ (accessed May 2, 2019).
(30) Clark, S. J.; Segall, M. D.; Pickard, C. J.; Hasnip, P. J.; Probert, M. I. J.; Refson, K.; Payne, M. C. First principles methods using CASTEP. *Z. Kristallogr. - Cryst. Mater.* **2005**, *220*, 567−570.
(31) Vanderbilt, D. Soft self-consistent pseudopotentials in a generalized eigenvalue formalism. *Phys. Rev. B: Condens. Matter Mater. Phys.* **1990**, *41*, 7892.
(32) Perdew, J. P.; Ruzsinszky, A.; Csonka, G. I.; Vydrov, O. A.; Scuseria, G. E.; Constantin, L. A.; Zhou, X.; Burke, K. Restoring the density-gradient expansion for exchange in solids and surfaces. *Phys. Rev. Lett.* **2008**, *100*, 136406.
(33) Tkatchenko, A.; Scheffler, M. Accurate Molecular Van Der Waals Interactions from Ground-State Electron Density and Free-Atom Reference Data. *Phys. Rev. Lett.* **2009**, *102*, 073005.
(34) Monkhorst, H. J.; Pack, J. D. Special points for Brillouin-zone integrations. *Phys. Rev. B* **1976**, *13*, 5188.
(35) Fall, C.; Binggeli, N.; Baldereschi, A. Deriving accurate work functions from thin-slab calculations. *J. Phys.: Condens. Matter* **1999**, *11*, 2689−2696.
(36) Heyd, J.; Scuseria, G. E. Assessment and validation of a screened Coulomb hybrid density functional. *J. Chem. Phys.* **2004**, *120*, 7274−7280.
(37) Hamann, D.; Schlüter, M.; Chiang, C. Norm-conserving pseudopotentials. *Phys. Rev. Lett.* **1979**, *43*, 1494.
(38) Rietveld, H. M. The rietveld method. *Phys. Scr.* **2014**, *89*, 098002.
(39) Glass, C. W.; Oganov, A. R.; Hansen, N. USPEX−Evolutionary crystal structure prediction. *Comput. Phys. Commun.* **2006**, *175*, 713−720.
(40) Shannon, R. D.; Prewitt, C. T. Revised values of effective ionic radii. *Acta Crystallogr., Sect. B: Struct. Crystallogr. Cryst. Chem.* **1970**, *26*, 1046−1048.
(41) Mattausch, H.; Eger, R.; Simon, A. Das erste Gadoliniumcarbidfluorid: Gd_2CF_2. *Z. Anorg. Allg. Chem.* **1991**, *597*, 145−150.
(42) Cockcroft, J. K.; Kremer, R. K.; Mattausch, H.; Raju, N. P.; Simon, A. Structure and magnetic ordering of holmium carbide fluoride, Ho_2CF_2. *J. Alloys Compd.* **1992**, *183*, 241−251.
(43) Come, J.; Naguib, M.; Rozier, P.; Barsoum, M. W.; Gogotsi, Y.; Taberna, P.-L.; Morcrette, M.; Simon, P. A non-aqueous asymmetric cell with a Ti_2C-based two-dimensional negative electrode. *J. Electrochem. Soc.* **2012**, *159*, A1368−A1373.
(44) Spanu, L.; Sorella, S.; Galli, G. Nature and Strength of Interlayer Binding in Graphite. *Phys. Rev. Lett.* **2009**, *103*, 196401.
(45) Druffel, D. L.; Kuntz, K. L.; Woomer, A. H.; Alcorn, F. M.; Hu, J.; Donley, C. L.; Warren, S. C. Experimental demonstration of an electride as a 2D material. *J. Am. Chem. Soc.* **2016**, *138*, 16089−16094.
(46) Kuntz, K. L.; Wells, R. A.; Hu, J.; Yang, T.; Dong, B.; Guo, H.; Woomer, A. H.; Druffel, D. L.; Alabanza, A.; Tománek, D.; Warren, S. C. Control of surface and edge oxidation on phosphorene. *ACS Appl. Mater. Interfaces* **2017**, *9*, 9126−9135.
(47) Poole, R. T.; Szajman, J.; Leckey, R. C. G.; Jenkin, J. G.; Liesegang, J. Electronic structure of the alkaline-earth fluorides studied by photoelectron spectroscopy. *Phys. Rev. B* **1975**, *12*, 5872−5877.
(48) Vasquez, R. XPS Core level spectra of some Y compounds. *J. Electron Spectrosc. Relat. Phenom.* **1990**, *50*, 167−170.
(49) Mongstad, T.; Thøgersen, A.; Subrahmanyam, A.; Karazhanov, S. The electronic state of thin films of yttrium, yttrium hydrides and yttrium oxide. *Sol. Energy Mater. Sol. Cells* **2014**, *128*, 270−274.
(50) Agarwal, M.; DeGuire, M. R.; Heuer, A. H. Synthesis of yttrium oxide thin films with and without the use of organic self-assembled monolayers. *Appl. Phys. Lett.* **1997**, *71*, 891−893.
(51) Ihara, H.; Kumashiro, Y.; Itoh, A. X-ray photoelectron spectrum and band structure of TiC. *Phys. Rev. B* **1975**, *12*, 5465.
(52) Ihara, H.; Hirabayashi, M.; Nakagawa, H. Electronic band structures and X-ray photoelectron spectra of ZrC, HfC, and TaC. *Phys. Rev. B* **1976**, *14*, 1707.
(53) Nyholm, R.; Berndtsson, A.; Martensson, N. Core level binding energies for the elements Hf to Bi (Z= 72−83). *J. Phys. C: Solid State Phys.* **1980**, *13*, L1091.
(54) Vasquez, R. P. SrF_2 by XPS. *Surf. Sci. Spectra* **1992**, *1*, 24−30.
(55) Padalia, B. D.; Gimzewski, J. K.; Affrossman, S.; Lang, W. C.; Watson, L. M.; Fabian, D. J. The reactions of oxygen and water with the rare-earth metals terbium to lutetium studied by x-ray photoelectron spectroscopy. *Surf. Sci.* **1976**, *61*, 468−482.
(56) Vasquez, R. P.; Foote, M. C.; Hunt, B. D. Reaction of nonaqueous halogen solutions with $YBa_2Cu_3O_{7-x}$. *J. Appl. Phys.* **1989**, *66*, 4866−4877.
(57) Nyholm, R.; Martensson, N. Core level binding energies for the elements Zr−Te (Z= 40−52). *J. Phys. C: Solid State Phys.* **1980**, *13*, L279.
(58) Zhang, C. J.; Pinilla, S.; McEvoy, N.; Cullen, C. P.; Anasori, B.; Long, E.; Park, S.-H.; Seral-Ascaso, A.; Shmeliov, A.; Krishnan, D.; Morant, C.; Liu, X.; Duesberg, G. S.; Gogotsi, Y.; Nicolosi, V. Oxidation stability of colloidal two-dimensional titanium carbides (MXenes). *Chem. Mater.* **2017**, *29*, 4848−4856.
(59) Li, G.; Jiang, K.; Zaman, S.; Xuan, J.; Wang, Z.; Geng, F. Ti_3C_2 sheets with an adjustable surface and feature sizes to regulate the chemical stability. *Inorg. Chem.* **2019**, *58*, 9397−9403.
(60) Wang, X.; Garnero, C.; Rochard, G.; Magne, D.; Morisset, S.; Hurand, S.; Chartier, P.; Rousseau, J.; Cabioc'h, T.; Coutanceau, C.; Mauchamp, V.; Célérier, S. A new etching environment (FeF_3/HCl) for the synthesis of two-dimensional titanium carbide MXenes: a route towards selective reactivity vs. water. *J. Mater. Chem. A* **2017**, *5*, 22012−22023.
(61) Chae, Y.; Kim, S. J.; Cho, S.-Y.; Choi, J.; Maleski, K.; Lee, B.-J.; Jung, H.-T.; Gogotsi, Y.; Lee, Y.; Ahn, C. W. An investigation into the factors governing the oxidation of two-dimensional Ti_3C_2 MXene. *Nanoscale* **2019**, *11*, 8387−8393.
(62) Lotfi, R.; Naguib, M.; Yilmaz, D. E.; Nanda, J.; van Duin, A. C. T. A comparative study on the oxidation of two-dimensional Ti_3C_2 MXene structures in different environments. *J. Mater. Chem. A* **2018**, *6*, 12733−12743.
(63) Huang, S.; Mochalin, V. N. Hydrolysis of 2D transition-metal carbides (MXenes) in colloidal solutions. *Inorg. Chem.* **2019**, *58*, 1958−1966.
(64) Alhabeb, M.; Maleski, K.; Mathis, T. S.; Sarycheva, A.; Hatter, C. B.; Uzun, S.; Levitt, A.; Gogotsi, Y. Selective etching of silicon from Ti_3SiC_2 (MAX) to obtain 2D titanium carbide (MXene). *Angew. Chem., Int. Ed.* **2018**, *57*, 5444−5448.
(65) Ghidiu, M.; Lukatskaya, M. R.; Zhao, M.-Q.; Gogotsi, Y.; Barsoum, M. W. Conductive two-dimensional titanium carbide 'clay' with high volumetric capacitance. *Nature* **2014**, *516*, 78.
(66) Zhang, W. L.; Deng, L.; Liu, J.; Liu, Y.; Yin, J.; Zeng, H.; Zheng, W.; Zhang, A. Unveiling the critical role of surface oxidation of electroresponsive behaviors in two-dimensional $Ti_3C_2T_x$ MXenes. *J. Phys. Chem. C* **2019**, *123*, 5479−5487.
(67) Khazaei, M.; Arai, M.; Sasaki, T.; Ranjbar, A.; Liang, Y.; Yunoki, S. OH-terminated two-dimensional transistion metal carbides and nitrides as ultralow work function materials. *Phys. Rev. B: Condens. Matter Mater. Phys.* **2015**, *92*, 075411.
(68) Schultz, T.; Frey, N. C.; Hantanasirisakul, K.; Park, S.; May, S. J.; Shenoy, V. B.; Gogotsi, Y.; Koch, N. Surface termination dependent work function and electronic properties of $Ti_3C_2T_x$ MXene. *Chem. Mater.* **2019**, *31*, 6590.

DOI: 10.1021/acs.chemmater.9b03722
Chem. Mater. XXXX, XXX, XXX−XXX